Atmos. Chem. Phys., 8, 4877–4889, 2008
www.atmos-chem-phys.net/8/4877/2008/

Atmospheric Chemistry and Physics

Direct detection of OH formation in the reactions of HO_2 with $CH_3C(O)O_2$ and other substituted peroxy radicals

T. J. Dillon and J. N. Crowley

Max-Planck-Institut für Chemie (Otto-Hahn-Institut) Joh.-Joachim-Becher-Weg 27, 55128 Mainz, Germany

Received: 6 March 2008 – Published in Atmos. Chem. Phys. Discuss.: 11 April 2008
Revised: 30 July 2008 – Accepted: 30 July 2008 – Published: 26 August 2008

Abstract. This work details the first direct observation of OH as a product from (R1): HO_2+$CH_3C(O)O_2$→(products), which has generally been considered an atmospheric radical termination process. The technique of pulsed laser photolysis radical generation, coupled to calibrated laser induced fluorescence detection was used to measure an OH product yield for (R1) of $\alpha_1(298\,\mathrm{K})=(0.5\pm0.2)$. This study of (R1) included the measurement of a rate coefficient $k_1(298\,\mathrm{K})=(1.4\pm0.5)\times10^{-11}\,\mathrm{cm^3\,molecule^{-1}\,s^{-1}}$, substantially reducing the uncertainties in modelling this important atmospheric reaction. OH was also detected as a product from the reactions of HO_2 with three other carbonyl-containing peroxy radicals, albeit at smaller yield, e.g. (R2): HO_2+$CH_3C(O)CH_2O_2$→(products), $\alpha_2\approx0.15$. By contrast, OH was not observed ($\alpha<0.06$) as a major product from reactions where carbonyl functionality was absent, e.g. HO_2+$HOCH_2CH_2O_2$ (R8), and HO_2+$CH_3CH(OH)CH_2O_2$ (R9).

1 Introduction

The hydroxyl radical, OH, is the primary oxidant in the Earth's atmosphere, initiating the degradation of common trace gases such as CH_4, CO and the important non-methane hydrocarbon (NMHC) isoprene (C_5H_8, 2-methyl-1,3-butadiene) (Atkinson and Arey, 2003). Key intermediates in the atmospheric oxidation of NMHC are the hydroperoxyl radical, HO_2, and organic peroxy radicals, RO_2 (Lightfoot et al., 1993; Tyndall et al., 2001). The reactions between HO_2 and RO_2 have long been of interest to atmospheric scientists as they are important radical termination processes, inhibiting O_3 and OH generation, and producing phytotoxic organic hydrogen peroxides, ROOH, and peracids, RC(O)OOH. Recent experimental and theoretical work has, however, suggested that the reactions of HO_2 with some substituted RO_2, do not exclusively terminate radical chemistry (Thornton et al., 2002). For the reaction (R1) of HO_2 with acetyl peroxyl, $CH_3C(O)O_2$, Hasson and co-workers reported a significant yield of OH radicals (R1c) (Hasson et al., 2004), in addition to the well-established radical terminating peracid (R1a) and O_3 (R1b) products (Niki et al., 1985; Moortgat et al., 1989; Horie and Moortgat, 1992; Crawford et al., 1999; Tomas et al., 2001).

$$HO_2+CH_3C(O)O_2 \rightarrow CH_3C(O)O_2H+O_2 \quad \text{(R1a)}$$

$$\rightarrow CH_3C(O)OH+O_3 \quad \text{(R1b)}$$

$$\rightarrow OH+CH_3C(O)O+O_2 \quad \text{(R1c)}$$

The OH or $CH_3C(O)O$ radical products (R1c) were not directly detected, but rather FTIR and HPLC end-product analysis (in particular of CH_3OOH produced in a series of reactions following $CH_3C(O)O$ decomposition) was used (Hasson et al., 2004) to derive an OH product yield, $\alpha_1\equiv k_{1c}/k_1=(0.4\pm0.16)$. The authors noted that OH generation in (R1c) may have caused a serious (factor of ≈2) underestimation in previous determinations of the overall rate coefficient, k_1. Depending on experimental conditions, the OH products could recycle HO_2 and $CH_3C(O)O_2$, essentially leaving kinetic experiments blind to (R1c).

Reaction (R1) was subsequently studied in two independent laboratories, both using an OH scavenger (benzene) to trap any OH products. From the results of new real-time experiments, a re-analysis of previously published kinetic data, and a theoretical treatment of (R1), Le Crâne et al. assigned an upper-limit of $\alpha_1<0.1$ (Le Crane et al., 2006) and concluded that (R1) is, as previously thought, predominantly a radical termination process. By contrast, Jenkin and co-workers did obtain evidence for a significant propagation

Correspondence to: T. J. Dillon
(dillon@mpch-mainz.mpg.de)

Published by Copernicus Publications on behalf of the European Geosciences Union.

(R1c) channel from their FTIR end-product analysis (Jenkin et al., 2007). Based largely upon yields of phenol (produced from C_6H_6+OH in air) Jenkin et al. obtained α_1=(0.43±0.1), in excellent agreement with the results of Hasson et al. It was suggested that Le Crâne et al. had overestimated the stability of HOC_6H_6 radicals (formed from C_6H_6+OH) used as the diagnostic for OH, and so underestimated the importance of channel (R1c). (Jenkin et al., 2007).

Note that none of these three studies (Hasson et al., 2004; Le Crane et al., 2006; Jenkin et al., 2007) could directly detect OH as product from (R1). Clearly there remain large uncertainties in both α_1 and k_1. The principal aim of the work presented in this manuscript was therefore to unambiguously identify any OH produced in (R1), and so to reduce uncertainties in the two important atmospheric parameters α_1 and k_1.

There are indications in the literature that other naturally occurring, substituted RO_2 may react with HO_2 to produce significant OH products. A large α_2=(0.69±0.2) was reported for the reaction (R2) of HO_2 with acetonyl peroxy, $CH_3C(O)CH_2O_2$ (Hasson et al., 2004):

$$HO_2+CH_3C(O)CH_2O_2 \rightarrow CH_3C(O)CH_2O_2H+O_2 \quad (R2a)$$

$$\rightarrow OH+CH_3C(O)CH_2O+O_2 \quad (R2b)$$

By contrast, no evidence for OH production was obtained from the reaction of HO_2 with the non-substituted $C_2H_5O_2$ radical. In a subsequent quantum chemical/master equation study, it was demonstrated that hydrogen bonding to the carbonyl group of $CH_3C(O)O_2$ or $CH_3C(O)CH_2O_2$ stabilises the hydrotetroxide intermediates that can lead to OH formation (Hasson et al., 2005). These findings led to speculation that structurally similar RO_2 may react with HO_2 to produce OH. At that time the only other results to support this contention was a large OH yield α=(0.76±0.04) from the reaction of HO_2 with $CF_3CF_2C(O)O_2$ (Andersen et al., 2003). Intriguingly, Hasson et al. also suggested that the necessary H-bonding stabilisation could be provided by RO_2 with hydroxyl functionality. This theoretical suggestion has found some support in the experimental observations of Jenkin et al. (2007) who reported a value of α_3=(0.20±0.05) from the reaction (R3) of HO_2 with the simplest hydroxy peroxy radical, $HOCH_2O_2$:

$$HO_2+HOCH_2O_2 \rightarrow HOCH_2O_2H+O_2 \quad (R3a)$$

$$\rightarrow HC(O)OH+H_2O+O_2 \quad (R3b)$$

$$\rightarrow OH+HOCH_2O+O_2 \quad (R3c)$$

Whilst (R1–R3) are atmospherically interesting and worthy of study in their own right, a host of more complex, substituted (carbonyl and/or hydroxyl containing) RO_2 are produced in the atmospheric oxidation of isoprene and other NMHC (Atkinson and Arey, 2003). If significant OH yields were found to be a general feature of HO_2+substituted RO_2 reactions, such chemistry would serious impact upon our understanding of atmospheric oxidation. The impact would be particularly large in remote regions, where low anthropogenic activity limits NO_x levels and suppresses radical propagation via (R4) and (R5):

$$HO_2+NO \rightarrow OH+NO_2 \quad (R4)$$

$$RO_2+NO \rightarrow RO+NO_2 \quad (R5)$$

For example, models predict small [OH] in air over tropical forests, due to rapid losses in reaction with isoprene (R6) and other NMHC, and the lack of verified mechanisms for OH regeneration from the hydroxy-RO_2 produced in (R7).

$$OH+C_5H_8 \rightarrow HOC_5H_8 \quad (R6)$$

$$HOC_5H_8+O_2 \rightarrow HOC_5H_8O_2 \quad (R7)$$

In a recent Max-Planck-Institute field campaign (GABRIEL), OH was for the first time directly monitored over the Amazonian rainforest (Lelieveld et al., 2008). The results (see elsewhere in this issue) clearly demonstrate that large [OH]$\approx 1\times10^7$ molecule cm^{-3} were maintained, despite a large (∼1 ppb) isoprene mixing ratio in otherwise clean air (NO ∼15 ppt). The largest discrepancies (up to a factor of 10) between measured and modelled [OH] were observed when isoprene mixing ratios were highest, indicating that our understanding of the (low NO_x) isoprene degradation mechanism is incomplete.

Accordingly, in this work the reactions of HO_2 with a variety of substituted RO_2 were studied, and any OH formed unambiguously identified by a direct OH detection technique. Careful calibration of the experiment allowed the determination of OH product yields (α) for the reactions of HO_2 with a variety of carbonyl-containing RO_2, including (R1) and (R2). For experimental reasons (see Sect. 3.4) it was not possible to investigate the RO_2 produced directly from isoprene (R6–R7), however, the reactions of HO_2 with several hydroxy-containing RO_2 were studied, notably (R8) with $HOCH_2CH_2O_2$: and (R9) with $CH_3CH(OH)CH_2O_2$.

$$HO_2+HOCH_2CH_2O_2 \rightarrow (\text{products}) \quad (R8)$$

$$HO_2+CH_3CH(OH)CH_2O_2 \rightarrow (\text{products}) \quad (R9)$$

2 Experimental

The experiments detailed in this work used Pulsed Laser Photolysis (PLP) generation of HO_2 and RO_2, coupled to direct, real-time observation of the product OH molecules by pulsed Laser Induced Fluorescence (LIF). Experiments were carried out "back-to-back" with chemical calibrations of the LIF system (see Sect. 2.4), which allowed conversion of fluorescence intensities into absolute [OH], and thus calculation of OH product yields (α).

2.1 The PLP-LIF technique

The PLP-LIF set-up used in these experiments has recently been used to study a number of OH reactions (Dillon et al., 2005; Dillon et al., 2006a; Dillon et al., 2007; Karunanandan et al., 2007). A detailed description including a schematic diagram of the apparatus was presented previously (Wollenhaupt et al., 2000), so only a brief description is given here. Experiments were conducted in a jacketed quartz reaction cell of volume $\approx$500 cm^3. Temperature in the cell was regulated by circulating a cryogenic fluid through the outer jacket, and monitored with a J-Type thermocouple situated close to the intersection of the photolysis and probe laser beams. Pressure was monitored with a 1300 mBar capacitance manometer. Gas flow rates, regulated using calibrated mass flow controllers, were between 1000 and 2000 cm^3 (STP) min^{-1}. The resulting linear gas velocities in the reaction cell ensured that a fresh gas sample was available for photolysis at each laser pulse (repetition rate 10 Hz), and so prevented a build up of products.

HO_2 and RO_2 radicals were generated from suitable precursors (see Sect. 2.3 below) by the $\approx$20 ns pulse of an exciplex laser (Lambda Physik, Lextra) operating at 351 nm (XeF). Fluorescence from OH product molecules was excited using the output from a Nd-YAG (Quantel) pumped dye laser (Lambda-Physik, using Rhodamine 6G dye), and detected by a photomultiplier tube shielded by 309 nm (interference) and BG 26 (glass cut-off) filters. Laser excitation spectra of OH (not displayed) with transitions consistent with other recently measured and calculated spectra were used to unambiguously identify OH. All quantitative experiments were conducted at a laser excitation wavelength of=281.997 nm, corresponding to the Q_1 (1) line in OH $A^2\Sigma$ (v=1)$\leftarrow$X$^2\Pi$ (v=0). Efficient quenching of the OH fluorescence by the bath gas (air) limited LIF sensitivity, which was measured (see Sect. 2.4) as [OH]$\approx 5\times10^9$ molecule cm^{-3} for signal:noise=1:1, averaging 10 laser pulses at P=200 mBar.

2.2 Reagent handling and concentration measurements

Liquid samples of the following organic reagents were subject to repeated T=77 K freeze-pump-thaw cycles prior to dilution in N_2 and storage in blackened glass bulbs: CH_3OH and C_2H_5OH (both Merck, 99.9%); CH_3CHO, $CH_3C(O)CH_3$, $(CH_3)_2CHOH$ and $C_2H_5C(O)CH_3$ (all Aldrich, 99.5%); C_6H_5CHO and $(CH_3)_2CHCH_2CH_2OH$ (both Merck, 99 %); and isoprene (Aldrich, 99%). NO (Linde) was distilled by repeatedly removing the light boiling fractions at T=77 K, and discarding the frozen residue as the sample was allowed to warm slowly. N_2 and O_2 (Messer 99.999%), and Cl_2 (Linde, 2.00% Cl_2 in 99.99% He) were used as supplied.

All reagent concentrations were determined by manometric methods to an estimated accuracy of $\pm$15%, based upon uncertainties in cylinder/bulb partial-pressures, calibrated mass flow rates, and absolute measurements of T and P. Where possible, online optical determinations of reagent concentration were used as an independent check on the manometric measurements. The simplest optical measurements monitored the absorption at 184.9 nm in a 43.8 cm long cell, situated downstream of the reaction cell. Briefly, the 184.9 nm line from a low-pressure Hg-lamp was isolated using an interference filter (185 nm, FWHM 10 nm, Oriel), passed through the gas mixture, and the transmitted intensity, I, recorded on a photodiode. A beam splitter allowed the simultaneous recording (on a reference photodiode) of incident light intensity, I_0. Literature values (in 10^{-19} cm^2 molecule^{-1}) of σ_X=6.65 and 11.8 (Dillon et al., 2005), 22.0 (Salahub and Sandorfy, 1971), and 30.1 (Gierczak et al., 2003) were used to determine concentrations for respectively X=CH_3OH, C_2H_5OH, $(CH_3)_2CHOH$ and $CH_3C(O)CH_3$ via the Beer-Lambert relationship, Eq. (1).

$$I = I_0 \exp\left(-\sigma_X \cdot [X] \cdot l\right) \quad (1)$$

These optical measurements were found to agree ($\pm$10%) with the manometric calculations, and thus verifying the consistency of mass flow controller calibrations etc.

A crucial parameter in all experiments was the concentration of the radical precursor Cl_2, which was measured by recording attenuation of (220$<$/nm$<$380 nm) light from a deuterium-lamp in a 30.0 cm cell, inserted serially upstream of the reaction cell. A 0.5 m monochromator (B&M Spektronik BM50, grating 300 lines blazed at 300 nm) collected the light and directed it onto a diode array detector (Oriel INSTAspec 2). Evaluated literature (Atkinson et al., 2007) cross-sections (e.g. $\sigma_{Cl_2}=2.55\times10^{-19}$ cm^2 at the maximum around 330 nm) , were used to obtain [Cl_2] (to an estimated accuracy of $\pm$10%) from fits of Eq. (1) to the recorded spectra.

2.3 Generation of HO_2 and RO_2

PLP of Cl_2 (R10) was used to initiate radical chemistry, generating Cl-atoms for conversion into both HO_2 and RO_2.

$$Cl_2 + h\nu(351\,\text{nm}) \rightarrow 2Cl \quad (R10)$$

Laser fluences of around 8 mJ cm^{-2} per pulse were used to generate an initial concentration of chlorine atoms, [Cl]$_0\approx 5\times10^{13}$ molecule cm^{-3}, calculated using a modified version Eq. (2) of the Beer-Lambert law:

$$[Cl]_0 = 2\frac{I_0 - I}{l} \text{ where } I = I_0 \exp\left(-\sigma \cdot [Cl_2] \cdot l\right) \quad (2)$$

where the evaluated literature cross-section of Cl_2 ($\sigma=1.9\times10^{-19}$ cm^2 at the photolysis wavelength λ=351 nm; Atkinson et al., 2007) and photolysis cell length (l=32 cm) were well-characterised. Under the optically thin conditions prevalent in these experiments, the incident light intensity I_0 (in photons cm^{-2}) was obtained from the incident laser

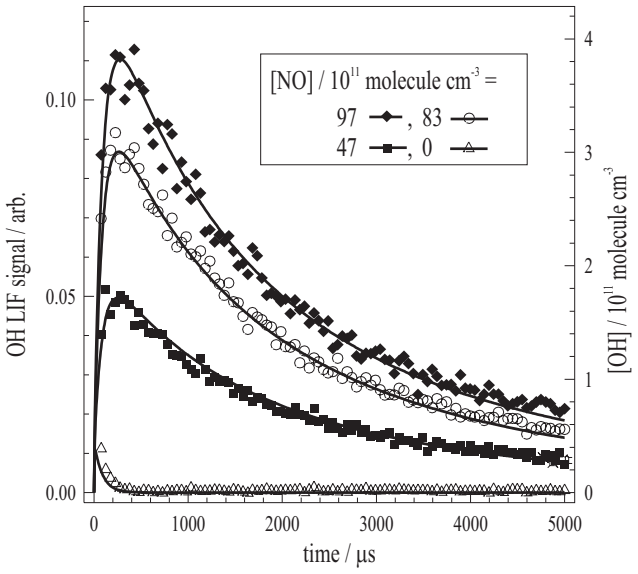

Fig. 1. Calibration of the OH LIF detection system using (R4) (HO_2+NO). Generation (R10–R12) of $[HO_2]=6.1\times10^{13}$ molecule cm^{-3} in the presence of $[NO]/10^{11}$ molecule cm^{-3}=97 (solid diamonds), 83 (open circles) and 47 (solid squares) produced these three OH profiles which were subsequently used to determine α_1 (see Fig. 2). Calibration was achieved by matching the LIF signal to that of its corresponding numerical simulation (see Sect. 2.4 for details).

fluence, measured using a joulemeter situated behind the photolysis cell. Corrections (20%) were made for the excimer beam divergence, and attenuation by the exit window. The joulemeter itself had been calibrated in previous work (Dillon et al., 2006b; Dillon et al., 2008). The errors in calculating $[Cl]_0$ by this method were estimated as 10% (precision) with an additional 30% (systematic error/accuracy) associated with imperfections in the photolysis beam profile, and overlap with the probe laser. The presence of large excess CH_3OH (see below) and O_2 (from the bath gas $P>100$ mBar of air) allowed the rapid conversion ($\tau<5\,\mu$s) of Cl to HO_2, and ensured that secondary radical chemistry from (R13) and (R14, α_{14}=0.21) (Atkinson et al., 2007) was minimised:

$$Cl+CH_3OH \rightarrow CH_2OH+HCl \quad (R11)$$

$$CH_2OH+O_2 \rightarrow HO_2+HCHO \quad (R12)$$

$$CH_2OH+Cl_2 \rightarrow ClCH_2OH+Cl \quad (R13)$$

$$Cl+HO_2 \rightarrow HCl+O_2 \quad (R14a)$$

$$\rightarrow ClO+OH \quad (R14b)$$

A small proportion of the Cl-atoms formed in (R10) were sequestered for peroxy radical production. In the study of (R1) for example, $CH_3C(O)O_2$ was generated by the addition of acetaldehyde, CH_3CHO, to the Cl_2/CH_3OH/air mixture:

$$Cl+CH_3CHO \rightarrow CH_3CO+HCl \quad (R15)$$

$$CH_3CO+O_2+M \rightarrow CH_3C(O)O_2+M \quad (R16a)$$

$$CH_3CO+O_2 \rightarrow OH+(\text{other products}) \quad (R16b)$$

$$CH_3CO+Cl_2 \rightarrow CH_3C(O)Cl+Cl \quad (R17)$$

Typical concentrations (in units of 10^{14} molecule cm^{-3}) of $[Cl_2]$=80 to 100, $[CH_3OH]$=40 to 180 and $[CH_3CHO]$=2 to 12 were chosen such that Cl was converted to $CH_3C(O)O_2$ and HO_2 within 2 μs. The amount of $CH_3C(O)O_2$ present in each experiment was controlled by the (well-characterised) relative rates of (R11) and (R15), and for the purposes of experimental planning/design could be estimated from Eq. (3):

$$\left[CH_3C(O)O_2\right] \approx [Cl]_0 \frac{k_{15}\,[CH_3CHO]\cdot(1-\alpha_{16})}{k_{15}\,[CH_3CHO]+k_{11}\,[CH_3OH]} \quad (3)$$

where the term (1–α_{16}) is close to unity in these experiments as OH production in (R16b) is efficient only at low pressures ($\alpha_{16}<0.1$ at all experimental $P>100$ mBar used here; Carr et al., 2007). In practice the majority (>80%) of the Cl produced in (R10) was used to generate HO_2. The resulting conditions of $[HO_2]>[RO_2]$, together with the slow and radical-terminating self-reaction (R18) of HO_2 ($k_{18}<3\times10^{-12}$ cm^3 molecule^{-1} s^{-1} at all experimental $P<1$ Bar used here) simplified data analysis and minimised unwanted radical generation in the fast, radical propagating (R19) ($k_{19}=1.6\times10^{-11}$ cm^3 molecule^{-1} s^{-1}; Atkinson et al., 2007).

$$HO_2+HO_2(+M) \rightarrow H_2O_2+O_2(+M) \quad (R18)$$

$$CH_3C(O)O_2+CH_3C(O)O_2 \rightarrow 2CH_3C(O)O+O_2 \quad (R19)$$

2.4 Calibration of the OH LIF detection system

LIF is a direct, but non-absolute technique, which meant that the detection system required calibration prior to conversion of OH fluorescence signals into absolute concentrations. A suitable calibration reaction was (R4), (HO_2+NO), as the yield of OH is known to be close to unity (α_4=0.984), and conveniently the rate coefficient ($k_4=8.9\times10^{-12}$ cm^3 molecule^{-1} s^{-1}; Atkinson et al., 2007) is similar to the rate coefficients for a number of HO_2+RO_2 reactions (e.g. $k_1=1.4\times10^{-11}$ cm^3 molecule^{-1} s^{-1}). Accordingly, small flows of NO were added to the Cl_2/CH_3OH/air photolysis mixture to generate well-characterised amounts of OH in conditions of P, $[Cl_2]$, $[CH_3OH]$, etc. as close as possible to those in the experiments to investigate (R1), i.e. with $[HO_2]>[NO]$ ($\approx[CH_3C(O)O_2]$).

Figure 1 displays the results of a series of calibration experiments, where three different measured [NO] (97, 83 and

47×10^{11} molecule cm^{-3}) were converted (R4) to OH by an excess [HO_2]=6.4×10^{13} molecule cm^{-3}. Calibration was achieved via numerical simulation of the data using the FACSIMILE program (Curtis and Sweetenham, 1987). Experimentally determined values of P, [Cl_2], [CH_3OH], [NO] and the laser fluence were used to initiate simulations, from which output values of [OH] were generated using the list of reactions and literature rate coefficients given in Appendix A. The relative position of the (arbitrary) LIF to the (absolute) [OH] y-axes was determined by scaling the OH LIF signals to their corresponding simulations. Calibration experiments were conducted prior to, between and after experiments to investigate (R1). The duration of a typical series of three calibrations interrupted by two experiments to determine α_1, was about 40 min, in which time fluctuations in LIF sensitivity were rarely significant.

The shapes of the OH profiles presented in Fig. 1 are initially counter-intuitive. Whilst OH is generated on the millisecond timescale of (R4), rapid loss processes, dominated by reactions (R20–21) with CH_3OH and HO_2, prevent [OH] from reaching its theoretical maximum value, which is equivalent to the parent [NO].

$$OH+CH_3OH \rightarrow H_2O+CH_2OH \quad \text{(R20)}$$

$$OH+HO_2 \rightarrow H_2O+O_2 \quad \text{(R21)}$$

For example, in Fig. 1 the open circle datapoints correspond to OH formed (R4) from [NO]=8.3×10^{12} molecule cm^{-3} at an approximate first-order rate k_4[HO_2]≈500 s^{-1}. OH is efficiently removed (k_{20}[CH_3OH]+k_{21}[HO_2]≈10 000 s^{-1}) before (R4) is complete, limiting the observed [OH] to a maximum value of ≈3×10^{11} molecule cm^{-3}. Note that all simulations adequately reproduced the shape of the OH decay profiles, which was controlled by the slower first-order rate of (R4), k_4[HO_2]. Since k_4 itself is well-known (Atkinson et al., 2007), it follows that calibration experiments such as those presented in Fig. 1 provide an independent validation of the values of [HO_2]=[Cl]–[$CH_3C(O)O_2$] calculated from Eqs. (2–3).

Potential systematic errors in the calibration process included interference from other fluorescing species, unwanted secondary OH production, and uncertainties in both (experimentally determined) reagent concentrations and the (literature) photochemical parameters used to simulate $[OH]_t$. Accordingly, experiments were conducted in which the probe laser was tuned away from the OH line (to λ=282.01 nm), whereupon no fluorescence was detected, indicating that OH and only OH contributed to the calibration profiles. Sensitivity analysis demonstrated that known secondary OH production, e.g. from (R14b) (HO_2+Cl→OH+ClO) was a negligible source of error. As is evident from the data recorded in the absence of NO (see Fig. 1, open triangle datapoints), LIF signals from (R14b) were small, and were removed within 300 μs (i.e. occurred on a completely different timescale to R4), and were anyway adequately accounted for in the simulations. As a result we consider the overall accuracy of the calibrations to be limited by uncertainties in reactant concentrations, particularly of NO (±15%), and the evaluated error in the most important rate parameter k_4, (±26% Atkinson et al., 2007) which when combined (in a squared sum) give an estimate for the overall uncertainty of ±30% for the calibration process.

3 Results and discussion

The experiments detailed in this work were conducted under conditions of [HO_2]>[RO_2]≈[NO], and as a result unwanted secondary radical generation was minimised. Nonetheless, the reaction mixtures were chemically quite complex, containing several radical species, including more than one potential source of OH. Analysis by conventional least-squares fitting techniques was therefore not applicable, and all results were obtained following numerical simulation of the data using the FACSIMILE program (Curtis and Sweetenham, 1987). Typically, experimental values of the laser fluence, P, [Cl_2], [CH_3OH], and concentration of RO_2 precursor e.g. [CH_3CHO] were used to initiate the simulations. Output values of t, [Cl], [HO_2], [RO_2], and [OH] were generated using the list of reactions and literature rate coefficients given in Appendix A.

3.1 HO_2+$CH_3C(O)O_2$→OH+other products, (R1)

3.1.1 Determination of OH yield α_1

Figure 2 displays the results of a typical experiment, conducted at T=298 K and P=229 mBar, to determine the yield α_1 of OH, formed in HO_2+$CH_3C(O)O_2$ (R1). The LIF signals were calibrated as described in Sect. 2.4. For clarity, only one calibration dataset (open black circles in Fig. 2 [NO]=8.3×10^{12} molecule cm^{-3}) is displayed here. The blue square datapoints show the LIF signal recorded following generation of [$CH_3C(O)O_2$]=7.0×10^{12} molecule cm^{-3} in the presence of [HO_2]=5.4×10^{13} molecule cm^{-3}. The LIF signal is of a comparable size to (factor of ≈2 smaller) and decays on a similar timescale to the calibration signal. In experiments where the probe laser was tuned away from the OH line (e.g. green square datapoints in Fig. 2 where λ=282.01 nm), no fluorescence was detected. These observations indicate that OH is indeed formed at significant yield from (R1).

More quantitative results were obtained by numerical simulation of the experiment. The solid red line that passes though the datapoints on Fig. 2 indicates the result of simulating the [$CH_3C(O)O_2$]=7.0×10^{12} molecule cm^{-3} (blue squares) experiment using α_1=0.5 and the recommended literature rate coefficient of k_1=1.4×10^{-11} cm^3 molecule^{-1} s^{-1} (Atkinson et al., 2007) The simulation reproduced the experiment well,

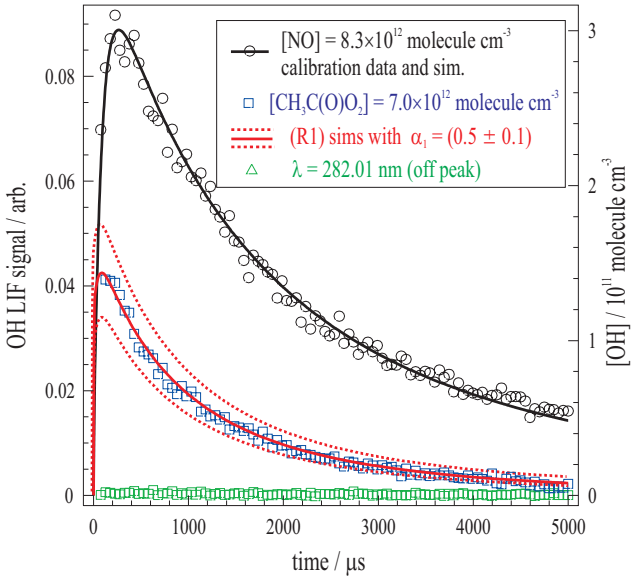

Fig. 2. Experiment to determine the yield of OH, α_1, for (R1) HO_2+$CH_3C(O)O_2$→(products). The blue squares show the OH LIF signal observed following generation of $[CH_3C(O)O_2]$=7.0×10^{12} molecule cm^{-3} in the presence of $[HO_2]$=5.4×10^{13} molecule cm^{-3}, clearly demonstrating that OH is a major product of (R1). Numerical simulations (in red) show that a yield of α≈0.5 was required to reproduce this and similar experimental datasets (see Table 1). Note that when the probe laser was tuned away from the OH line (λ=282.01 nm, green squares), no fluorescence was detected, indicating that OH and only OH was detected as a product from (R1). These LIF signals were calibrated (R4) using the data presented in Fig. 1. For clarity only one calibration profile is displayed here (open black circles: [NO]=8.3×10^{12} molecule cm^{-3}).

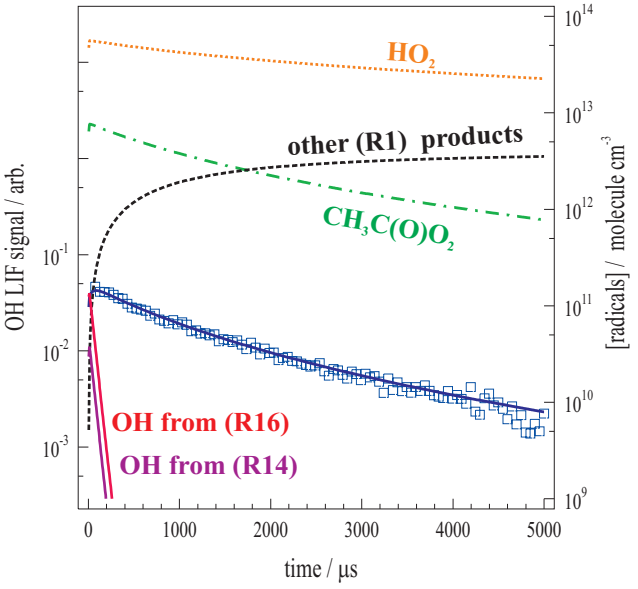

Fig. 3. Numerical simulation of an experiment to determine α_1 (note the logarithmic scale on the y-axes). In blue are the experimental datapoints already displayed in Figure 2, with corresponding simulation using α_1=0.5. OH profiles resulting from (R14b) and (R16b), simulated here as purple and red solid lines, have very different temporal characteristics to (R1). These reactions were not therefore a major source of error in our determination of α_1=0.5.

and was particularly sensitive to α_1, as is demonstrated in Fig. 2 where simulations (red dotted-lines) using α_1=0.4 and α_1=0.6 are also displayed. The overall accuracy of our determination of α_1 was however governed by systematic uncertainties associated with the LIF calibration, and parameters used in the simulations. Errors associated with secondary radical production, including other known sources of OH, were assessed, but found to be insignificant. Figure 3 displays the full output of the same simulation, including profiles of $[HO_2]$, $[CH_3C(O)O_2]$, [OH] and other products of (R1), on logarithmic scale. The simulation shows that a large excess of HO_2 was maintained throughout the experiment, ensuring that (R1) was the principal fate for $CH_3C(O)O_2$. Both (R14b) (Cl+HO_2) and (R16b) (CH_3CO+O_2) were known to be minor secondary sources of OH in these experiments. Nonetheless, as was shown by the open triangles data in Fig. 1, the maximum ($[CH_3CHO]$=0) impact of (R14b) was small. The contributions of (R14b) and (R16b) were assessed individually by simulation, as presented in Fig. 3. Both reactions occur on a much shorter timescale than (R1), and because of the short chemical lifetime of OH in these experiments, their contribution to the overall [OH] observed was negligible after about 100 μs.

Table 1 lists the conditions and results of all experiments to study (R1). A set of experiments (corresponding to one row in Table 1) generally consisted of determinations of α_1 from two or more different $[CH_3C(O)O_2]$, generated by changing the parent CH_3CHO concentration. Conditions of P, T and reagent concentrations were otherwise unchanged. Note that values of $[HO_2]$ were not listed explicitly as these changed slightly from the calibration (where $[HO_2]$≈$[Cl]_0$) to the (R1) experiments (where $[HO_2]$≈$[Cl]_0$–$[CH_3C(O)O_2]$). New calibration data was required for experiments conducted at different P, as the LIF detection sensitivity was strongly influenced by fluorescence quenching by the bath gas (air). There was no systematic change in the α_1≈0.5 required to simulate experimental observations, which were obtained over a range pressures (100–705 mBar) and at around ambient T. The range of precursor concentrations was necessarily limited so as to minimise secondary chemistry e.g. in (R13–14), (R16b–17) and (R18–R19), whilst maintaining a suitable millisecond timescale for (R1). The uncertainties in α_1 quoted in Table 1 refer to the internal consistency of the calibration and α_1 data (i.e. data from Fig. 2 listed as α_1=(0.5±0.05) as we can distinguish it from α_1=0.4 or 0.6).

Table 1. Determinations of α_1(298 K) and corresponding experimental conditions.

P/mBar	$[CH_3OH]$ [a]	$[CH_3CHO]$ [a]	$[Cl_2]$ [a]	[Cl] [b]	m, [NO] [b]	n, $[CH_3C(O)O_2]$ [b]	α_1^c
100	49.0	1.8–3.4	89	580	4, 29–61	3, 29–52	0.55±0.10
207	9.6	0.7	72	440	2, 120	2, 39	0.45±0.10
229	60.8	3.0–5.7	92	610	3, 47–97	2, 39–70	0.5±0.05
230	44.2	1.9–5.0	98	720	4, 27–69	3, 30–72	0.55±0.05
240	33.0	1.7–3.0	86	640	2, 42	2, 43–75	0.55±0.05
250	32.3	1.2–3.2	91	640	4, 17–44	4, 30–76	0.5±0.05
430	41.0	1.6–4.8	78	550	4, 26–67	3, 28–80	0.6±0.15
705	95.1	6.1–8.5	96	590	2, 58–149	2, 47–68	0.45±0.10

notes: [a]= precursor concentrations in units of 10^{14} molecule cm^{-3};
[b]= radical (Cl, NO, $CH_3C(O)O_2$) concentrations in units of 10^{11} molecule cm^{-3};
m= number of calibration (R4) profiles recorded, over a range of [NO];
n= number of (R1) profiles used to determine α_1;
[c]= errors in α_1 account for variability in (R1) or calibration data and do not include the systematic uncertainty (±25%) in initial radical density – see Sect. 3.1 for details.

A weighted average (using these precision-only errors) of the data in Table 1 gives α_1=(0.52±0.02). A more realistic assessment of the overall uncertainty in α_1 was obtained by combining this statistical error with the LIF calibration uncertainty (±30%, see Sect. 2.4), and errors associated with the simulations of (R1). Note that since these experiments were conducted back-to-back with the LIF calibrations, errors associated with a number of important parameters (e.g. $[HO_2]$, OH lifetime, P, T) cancelled-out, and could be neglected when assessing the overall uncertainty in α_1. Sensitivity analysis identified the remaining critical parameters as those controlling the concentration of parent radicals, $[CH_3C(O)O_2]$, and the rate coefficient for conversion to OH, k_1. Uncertainties in: laser fluence (±20%); $[Cl_2]$ (±10%); relative $[CH_3CHO]$ to $[CH_3OH]$ (±10%); rate coefficients k_{15} and k_{11} (relative rate measured both relative to C_2H_6 and C_2H_4 to about ±5%; Tyndall et al., 1999) were therefore combined to give an overall estimate of ±25% in $[CH_3C(O)O_2]$. This value was combined with an effective uncertainty in k_1 (±15%, see Sect. 3.1.2 below) and that of the LIF calibration process (±30%), to obtain an overall estimated accuracy of 40%, or α_1=(0.5±0.2).

3.1.2 Determination of the rate coefficient k_1, and uncertainties therein

All values of α_1 listed in Table 1 were obtained from simulations using the evaluated literature rate coefficient k_1(298 K)=1.4×10^{-11} cm^3 molecule^{-1} s^{-1}, which was based upon the results of two laboratory studies (Moortgat et al., 1989; Tomas et al., 2001). A large uncertainty of approximately a factor of two is quoted (Atkinson et al., 2007) to account for possible systematic errors. LIF detection of OH, used to monitor (R1) in this work, allowed for a more precise value of k_1(298 K) to be determined, as many of the problems associated with earlier studies were avoided. Firstly, LIF is a more selective technique than the monitoring of overlapping UV absorptions from HO_2 and $CH_3C(O)O_2$, used in the earlier kinetic studies (Moortgat et al., 1989; Tomas et al., 2001). Second, LIF is also more sensitive than conventional absorption techniques, allowing smaller radical concentrations to be used. As a result, the experiments could be conducted under kinetic conditions which minimised unwanted radical losses (see below).

With reference to Fig. 3, retrieval of k_1 was aided by having one reagent (HO_2, orange dotted line) in large excess over the course of the experiment. As a result the kinetic profile was (to a first approximation) governed by $[HO_2]$ and k_1. OH has a very different time profile to the other products of (R1), and in effect acts as a "spectroscopic marker" for its parent radical $CH_3C(O)O_2$ (green dot-dashed line). Simulations which used k_1 values at the upper or lower limits of the recommendation (2.8×10^{-11} and 7×10^{-12} cm^3 molecule^{-1} s^{-1}) were not consistent with any data recorded in this work. Simulations using (1.1<k_1<1.7)×10^{-11} cm^3 molecule^{-1} s^{-1} were able to reproduce the data (whilst adjusting α_1±20%) within the noise. It was this uncertainty of ±20% in k_1 which propagates into the overall error in α_1, as systematic errors in $[HO_2]$ were also present in the back-to-back calibrations (R4) experiments.

Secondary radical processes, which occurred in the earlier studies (Moortgat et al., 1989; Tomas et al., 2001), were of little consequence here. Sensitivity analysis demonstrated that the $CH_3C(O)O_2$ self-reaction (R19) accounted for less than 12% of the $CH_3C(O)O_2$ loss rate under all conditions. Inclusion of the equilibrium process (R22) had no discernable impact on the simulations as relatively small

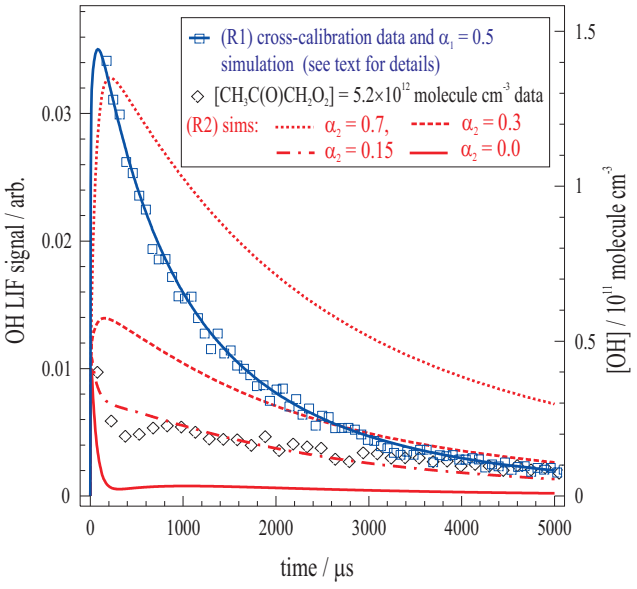

Fig. 4. Experiment to determine the OH yield α_2 for (R2) HO_2+$CH_3C(O)CH_2O_2$→(products). The black diamonds represent the OH LIF signal recorded following generation of $[CH_3C(O)CH_2O_2]$=5.2×10^{12} molecule cm^{-3} in the presence of $[HO_2]$=5.8×10^{13} molecule cm^{-3}. LIF was calibrated by the regular (R4) method (see section 2.4). Note that the apparent dip in the LIF signal at t∼400 μs was absent in similar (R2) datasets. Back-to-back experiments were also conducted where $CH_3C(O)$ CH_3 was replaced by CH_3CHO, and the OH yields from (R2) and (R1) were directly compared. The result (blue square datapoints and solid line depicting α_1=0.5) confirms that α_2 is indeed significantly smaller than α_1.

$[CH_3CHO]<1\times10^{15}$ molecule cm^{-3} were used in this work.

$$HO_2+CH_3CHO \leftrightarrow CH_3C(OH)O_2 \quad \text{(R22)}$$

That OH was not then recognised as a significant product of (R1) introduces the largest uncertainty into earlier k_1 determinations (Atkinson et al., 2007). Recycling of reactants via the reactions of OH with CH_3OH (R20) and CH_3CHO (R23), was not accounted for in previous analyses (Moortgat et al., 1989; Tomas et al., 2001), as no production of OH in (R1) was anticipated.

$$OH+CH_3CHO \rightarrow CH_3CO+H_2O \quad \text{(R23)}$$

In this work regeneration of HO_2 was of no consequence, as this reagent was in excess, whilst regeneration of CH_3CO in (R23) was kept to a minimum (in all experiments <20%) by the use of small $[CH_3CHO]$.

We conclude that, whilst these experiments were designed primarily to determine α_1, the high selectivity and sensitivity of the OH LIF detection technique has allowed the uncertainties in k_1(298 K) to be reduced. The principal source of error in these determinations was the ±30% uncertainty in $[HO_2]$, which when added to statistical errors results in an absolute value of k_1(298 K)=(1.4±0.5)×10^{-11} cm^3 molecule^{-1} s^{-1}. We note that uncertainties in this parameter could be further reduced if the excess reagent HO_2 was monitored, in addition to OH.

3.2 HO_2+$CH_3C(O)CH_2O_2$→products, (R2)

Photolysis (R10) of Cl_2 in the presence of acetone, $CH_3C(O)CH_3$, was used to generate acetonyl peroxy radicals for the investigation of (R2) (HO_2+$CH_3C(O)CH_2O_2$).

$$Cl+CH_3C(O)CH_3 \rightarrow CH_3C(O)CH_2+HCl \quad \text{(R24)}$$

$$CH_3C(O)CH_2+O_2+M \rightarrow CH_3C(O)CH_2O_2+M \quad \text{(R25)}$$

Similar methods to those detailed above were used to simultaneously generate an excess of HO_2 (R11–12), see Sect. 2.3, and to calibrate the OH LIF signals (see Sect. 2.4). The black diamonds datapoints in Fig. 4 represent the $[OH]_t$ obtained at P=230 mBar from $[CH_3C(O)CH_2O_2]$=5.2×10^{12} molecule cm^{-3} in the presence of $[HO_2]$=5.8×10^{13} molecule cm^{-3}. It was apparent from this and similar datasets (see Table 2 for details) that the yield of OH from (R2) was considerably smaller than the literature value (Hasson et al., 2004) of α_2=(0.67±0.20). Numerical simulation of the data using the list of reactions in Appendix A, and α_2=0.7 generated $[OH]_t$ profiles (e.g. red-dotted line in Fig. 4) that grossly overestimated every experimental observation. A significant $\alpha_2>0$ was nonetheless required to adequately simulate the data, with $\alpha_2 \approx 0.15$ (e.g. the dot-dashed line in Fig. 4) giving best results.

Such a large discrepancy between the results of this work, and those obtained by Hasson et al. was a source of concern. As a check on the reliability and reproducibility of the PLP/calibrated-LIF method used in this work, back-to-back experiments were conducted where $CH_3C(O)CH_3$ was replaced by a kinetically equivalent amount of CH_3CHO (i.e. $k_{15}[CH_3CHO] \approx k_{24}[CH_3C(O)CH_3]$). The OH produced in (R2) and (R1) could then be compared directly. Such relative yield experiments do not rely exclusively upon LIF calibration in (R4), and as such were useful as a double-check on laser alignment etc. The blue square datapoints in Fig. 4 display the resulting OH profile from (R1), which indicates that $\alpha_1 \gg \alpha_2$, again in contrast to the literature results (Hasson et al., 2004).

One difference between the (R2) and (R1) experiments was the use of considerably larger $[CH_3C(O)CH_3]$ (∼10^{16} molecule cm^{-3}, see Table 2) than $[CH_3CHO]$ (<10^{15} molecule cm^{-3}) to generate similar concentrations of RO_2. This was an unavoidable result of differences in reactivity towards Cl (in 10^{-12} cm^3 molecule^{-1} s^{-1}: k_{24}=2.1 whereas k_{15}=80). Changes in LIF sensitivity due to physical quenching were not anticipated, as in these experiments O_2 (20% of the bath gas), was always present in large excess, and is an efficient quencher of

Table 2. Determinations of OH yield α for other HO_2+RO_2 reactions.

HO_2 +	RH	[RH] [a]	n, [RO_2] [b]	α [c]
$CH_3C(O)CH_2O_2$ (R2)	$CH_3C(O)CH_3$	32–360	6, 14–110	0.15±0.1
$HOCH_2CH_2O_2$ (R8)	CH_3CH_2OH [d]	29–40	6, 51–53	< 0.04
$CH_3CH(OH)CH_2O_2$ (R9)	$(CH_3)_2CHOH$	4.9–9.6	2, 12–20	< 0.06
$ClC_5H_8O_2$ (R33) [e]	C_5H_8	0.54	1, 43	< 0.04
$HOC_5H_{10}O_2$ (R34) f	$(CH_3)_2CH(CH_2)_2OH$	0.6–1.2	3, 14–26	< 0.06
$C_6H_5C(O)O_2$ (R35)	C_6H_5CHO	2.0–3.9	2, 47–87	≈ 0.2
$C_2H_5C(O)CH_2O_2$ (R36) [g]	$CH_3C(O)C_2H_5$	8.1–11.5	3, 55–76	≈0.2

notes: all experiments conducted at around T=298 K and P=220 mBar unless stated, see Sect. 3.4 for further details;
[a]= [RH] in units of 10^{14} molecule cm^{-3};
[b]= n is number of determinations of α, [RO_2] in units of 10^{11} molecule cm^{-3};
[c]= errors in α do not include the systematic uncertainty (±25%) in initial radical density;
[d]= α_8 determined at T=259, 298 and 351 K;
[e]= $ClC_5H_8O_2$ refers to 4 isomeric RO_2; f=$HOC_5H_{10}O_2$ refers to three isomers;
[g]= $C_2H_5C(O)CH_2O_2$ refers to three isomers.

OH (k_Q=1.4×10^{-10} cm^3 molecule^{-1} s^{-1}; Bailey et al., 1997). Nonetheless, it was thought prudent to directly monitor the OH LIF response to the presence of such large [$CH_3C(O)CH_3$] in experiments using H_2O_2 photolysis (R26) as a direct, well-characterised source of OH.

$$H_2O_2 + h\nu(248\,\text{nm}) \rightarrow 2OH \quad \text{(R26)}$$

$$OH + CH_3C(O)CH_3 \rightarrow H_2O + CH_3C(O)CH_2 \quad \text{(R27)}$$

No $CH_3C(O)CH_3$ mediated quenching of the OH LIF signals was observed. In the course of these experiments, the rate coefficient k_{27}=(1.9±0.2)×10^{-13} cm^3 molecule^{-1} s^{-1} was obtained, in good agreement with the evaluated literature (k_{27}=(1.8±0.4)×10^{-13} cm^3 molecule^{-1} s^{-1}; Atkinson et al., 2007) thereby increasing confidence in the supply of acetone, and the (R2) reaction system.

It was difficult to obtain more information about (R2), as the only species detected (OH) was produced at such small yield. Simulations were generally initiated using the evaluated literature value of k_2(298 K)=9.0×10^{-12} cm^3 molecule^{-1} s^{-1}. This recommendation is based on the results of just one experimental study (Bridier et al., 1993), and is consequently quoted with an uncertainty of approximately a factor of 2. An improved reproduction of the data was achieved (e.g. in Fig. 4) when values close to the lower error limit for k_2 of 5×10^{-12} cm^3 molecule^{-1} s^{-1} were used. However, given that OH is produced via (R1) which follows the break-up (R28) of $CH_3C(O)CH_2O$ (a product of R2) and rapid conversion (R16) of CH_3CO to $CH_3C(O)O_2$, Bridier et al. should have underestimated k_2.

$$CH_3C(O)CH_2O \rightarrow CH_3CO + HCHO \quad \text{(R28)}$$

Secondary OH production in this reaction system is, however quite difficult to quantify, as losses of $CH_3C(O)CH_2O_2$ include (R29) which also produces $CH_3C(O)CH_2O$ and ultimately OH.

$$CH_3C(O)CH_2O_2 + CH_3C(O)CH_2O_2 \rightarrow 2CH_3C(O)CH_2O + O_2 \quad 60\% \quad \text{(R29a)}$$

$$\rightarrow CH_3C(O)CH_2OH + CH_3C(O)CHO + O_2 \quad 40\% \quad \text{(R29b)}$$

Approximately equal amounts of HO_2 and RO_2 were used in the earlier kinetic study (Bridier et al., 1993), leading to near 50% of initial $CH_3C(O)CH_2O_2$ reacting via (R29) rather than (R2). Similarly, in the experiments of Hasson et al. a significant proportion (>30%) of $CH_3C(O)CH_2O_2$ was lost in (R29). Subsequent OH formation from the reaction sequence (R29a), (R28), and (R1) was included in their analysis (Hasson et al., 2004), though it is unclear how sensitive their result of α_2=(0.67±0.2) is to the values of k_2 and k_{29} used. Note that due to the experimental conditions of [HO_2]>[$CH_3C(O)CH_2O_2$] used in this work, (R2) accounted for >90% of $CH_3C(O)CH_2O_2$ loss. Secondary OH production via (R29a), (R28), (R16) and (R1) was therefore minimised. We are confident therefore in the result of α_2=(0.15±0.10) obtained in this work, which agrees well with a recent determination of α_2=(0.15±0.08) from (Jenkin et al., 2008). Note however that inconsistencies remain in the values of k_2 used here and those of Bridier et al. Further experiments in which HO_2, $CH_3C(O)CH_2O_2$ and OH were monitored would help to resolve these issues.

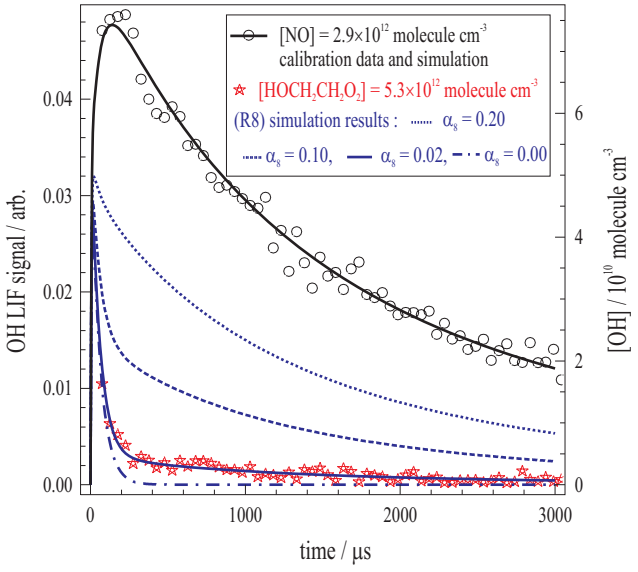

Fig. 5. Experiment to determine α_8 for (R8) HO_2+$HOCH_2CH_2O_2$→(products). The open black circles describe data where [NO]=2.9×10^{12} molecule cm^{-3} was used to generate a known amount of OH and hence calibrate the LIF detection system. The red stars show data obtained following generation of [$HOCH_2CH_2O_2$]=5.3×10^{12} molecule cm^{-3} in the presence of [HO_2]=5.6×10^{13} molecule cm^{-3}. Numerical simulation demonstrated that small OH yields of $\alpha_8\approx0.02$ were required to reproduce this and similar datasets (see section 3.3 and Table 2 for details).

3.3 The reaction (R8) HO_2+$HOCH_2CH_2O_2$→ (products)

Photolysis (R10) of Cl_2 in the presence of ethanol was used to generate a simple hydroxyperoxy radical, $HOCH_2CH_2O_2$, and HO_2:

$$Cl+CH_3CH_2OH \rightarrow CH_3CHOH+HCl \quad 92\% \qquad \text{(R30a)}$$

$$\rightarrow CH_2CH_2OH \quad 8\% \qquad \text{(R30b)}$$

$$CH_3CHOH+O_2 \rightarrow HO_2+CH_3CHO \qquad \text{(R31)}$$

$$CH_2CH_2OH+O_2+M \rightarrow HOCH_2CH_2O_2+M \qquad \text{(R32)}$$

Conveniently, the reaction sequence (R30–32) produced the large excess of [HO_2]>[$HOCH_2CH_2O_2$] required to determine α_8. As a result these experiments were conducted in the absence of CH_3OH. Figure 5 displays the results of one such experiment conducted at T=298 K and P=250 mBar. The open black circles describe data where [NO]=2.9×10^{12} molecule cm^{-3} was used to generate (R4) a known amount of OH and hence calibrate the LIF detection system. The red stars show the comparatively small amount of OH generated from [$HOCH_2CH_2O_2$]=5.3×10^{12} molecule cm^{-3} in the presence of [HO_2]=5.6×10^{13} molecule cm^{-3}. Numerical simulation using the recommended k_8=1.2×10^{-11} cm^3 molecule^{-1} s^{-1} (Atkinson et al., 2007), demonstrated that small OH yields of $\alpha_8\approx0.02$ were required to reproduce this and similar datasets (see Table 2). To account for uncertainties particularly in k_8 (±60%) we quote a conservative upper-limit of $\alpha_8<0.04$. Similar results were obtained at T=257 and 351 K.

3.4 OH yields for other HO_2+RO_2 reactions

The methods detailed in Sect. 2 were used to measure OH product yields for the reactions of a number of other substituted peroxy radicals with HO_2. Common to each system studied was PLP generation (R10) of [Cl]=7×10^{13} molecule cm^{-3}, in the presence of [CH_3OH]=6×10^{15} molecule cm^{-3} and P=220 mBar (air) to facilitate formation (R11–12) of the excess reagent HO_2. The OH LIF system was calibrated using HO_2+NO (R4), as described in Sect. 2.4. Note that simulation of the observed OH profiles relied upon a host of kinetic data (see Appendix A), which was not completely available. Crucially, no literature rate coefficients for the HO_2+RO_2 reactions were found, therefore an estimated value of k=1×10^{-11} cm^3 molecule^{-1} s^{-1} was adopted for all such processes. As a result, the values of α listed in Table 2 (excepting α_2 and α_8) should be regarded as no more than semi-quantitative.

No evidence for OH production was observed upon addition of $(CH_3)_2CHOH$ to the Cl_2/CH_3OH/air photolysis mixture for the study of (R9) (HO_2+$CH_3CH(OH)CH_2O_2$). Following consideration of the noise on the LIF signals, and uncertainties in the estimated value of k_9=1×10^{-11} cm^3 molecule^{-1} s^{-1} used, a conservative upper-limit of $\alpha_9<0.06$ was assigned. It was unfortunately not possible to investigate RO_2 generated from unsaturated precursors, such as the atmospherically important hydroxyperoxy radicals produced (R6–7) from isoprene. Addition of isoprene to the Cl_2/CH_3OH/air photolysis mixture produced a mixture of $C_5H_8ClO_2$ isomers in an excess of HO_2, from which no OH was observed ($\alpha_{33}<0.03$, see Table 2).

$$HO_2+ClC_5H_8O_2 \rightarrow \text{(products)} \qquad \text{(R33)}$$

Addition of isopentanol to the photolysis mixture was used to generate structurally similar (saturated) analogues of the target isoprene hydroxyperoxys. No OH production was observed however, and an upper-limit of $\alpha_{34}<0.06$ was derived.

$$HO_2+HOC_5H_{10}O_2 \rightarrow \text{(products)} \qquad \text{(R34)}$$

By contrast, strong evidence for OH formation was observed ($\alpha\approx0.2$) for the reactions of HO_2 with RO_2 containing a carbonyl group, e.g. those from benzaldehyde and butanone:

$$HO_2+C_6H_5C(O)O_2 \rightarrow OH+\text{(otherproducts)} \qquad \text{(R35)}$$

$$HO_2+(C_4H_7O)O_2 \rightarrow OH+\text{(other products)} \qquad \text{(R36)}$$

4 Atmospheric implications and conclusions

OH was, for the first time, directly observed as a product from reactions of HO_2 with peroxy radicals. For the reaction (R1) (HO_2+$CH_3C(O)O_2$), an OH product yield α_1=(0.5±0.2) was measured, in good agreement with two recent indirect determinations (Hasson et al., 2004; Jenkin et al., 2007). The rate coefficient k_1(298 K)=(1.4±0.5)×10^{-11} cm^3 $molecule^{-1}$ s^{-1}, was determined, substantially reducing the uncertainties in this important atmospheric parameter. OH products were also observed from the reactions of HO_2 with three other carbonyl-containing RO_2 (produced from acetone, benzaldehyde and butanone). These results imply that a host of HO_2+carbonyl-RO_2 reactions, previously considered to be radical-terminating, may produce OH in the atmosphere. For (R2) (HO_2+$CH_3C(O)CH_2O_2$) the measured α_2 ≈0.15 was considerably smaller than in the only literature determination (Hasson et al., 2004). By contrast OH was not observed as a major product from reactions where carbonyl functionality was absent, e.g. the reactions of HO_2 with hydroxy-containing RO_2. Conservative upper-limits were assigned for the reactions of HO_2 with $HOCH_2CH_2O_2$ (R8, α_8<0.05), $CH_3CH(OH)CH_2O_2$ (R9, α_9<0.06) and $HOC_5H_{10}O_2$ (R34, α_{34}<0.06).

Appendix A

List of reactions and rate parameters used in data simulations.

(R11)	$Cl+CH_3OH \rightarrow CH_2OH$	5.5×10^{-11}	
(R14a)	$Cl+HO_2 \rightarrow$	$(1–1.7\exp(–620/T)) \times 4.4\times10^{-11}$	
(R14b)	$Cl+HO_2 \rightarrow OH+ClO$	$1.7\exp(–620/T)\times 4.4\times10^{-11}$	
(R12)	$CH_2OH+O_2 \rightarrow HO_2+HCHO$	9.7×10^{-12}	
	$CH_3O+O_2 \rightarrow HO_2+HCHO$	$7.4\times10^{-14}\exp(–1080/T)$	
(R13)	$CH_2OH+Cl_2 \rightarrow Cl$	2.9×10^{-11}	(Tyndall et al., 1999)
(R4)	$HO_2+NO \rightarrow OH+NO_2$	$3.6\times10^{-12}\exp(270/T)$	
(R18)	$HO_2+HO_2 \rightarrow$	$2.2\times10^{-13}\exp(600/T)+1.9\times10^{-33}[M]\exp(980/T)$	
(R20a)	$OH+CH_3OH \rightarrow CH_2OH$	$0.85\times6.38\times10^{-5}T^2\exp(144/T)$	
(R20b)	$OH+CH_3OH \rightarrow CH_3O$	$0.15\times6.38\times10^{-5}T^2\exp(144/T)$	
(R21)	$OH+HO_2 \rightarrow$	$4.8\times10^{-11}\exp(250/T)$	
	$OH+NO+M \rightarrow$	k_0=7.4×10^{-31} [N_2], k_∞=3.3×10^{-11}, Fc=0.81	
	$ClO+NO \rightarrow Cl$	$6.2\times10^{-12}\exp(295/T)$	
	$ClO+HO_2 \rightarrow$	$2.2\times10^{-12}\exp(340/T)$	
(R15)	$Cl+CH_3CHO \rightarrow CH_3CO$	8.0×10^{-11}	
(R16a)	$CH_3CO+O_2 \rightarrow CH_3C(O)O_2$	$(1-\alpha_{16})\times5.1\times10^{-12}$	
(R16b)	$CH_3CO+O_2 \rightarrow OH$	$\alpha_{16}\times5.1\times10^{-12}$	
(R17)	$CH_3CO+Cl_2 \rightarrow Cl$	4.3×10^{-11}	(Tyndall et al., 1999)
(R22)	$HO_2+CH_3CHO \leftrightarrow CH_3C(OH)O_2$	k_{22}=4.4×10^{-14}, K_{22}=$1.9\times10^{-27}\exp(6925/T)$ cm^3 $molecule^{-1}$.	(Tomas et al., 2001)
(R23)	$OH+CH_3CHO \rightarrow CH_3CO$	$4.4\times10^{-12}\exp(365/T)$	
(R1c)	$CH_3C(O)O_2+HO_2 \rightarrow OH+CH_3$	$k_1\times\alpha_1$	(varied, this work)
(R1ab)	$CH_3C(O)O_2+HO_2 \rightarrow$	$k_1\times(1–\alpha_1)$	(varied, this work)
(R19)	$CH_3C(O)O_2+CH_3C(O)O_2 \rightarrow 2CH_3$	$2.9\times10^{-12}\exp(500/T)$	
(R2a)	$HO_2+CH_3C(O)CH_2O_2 \rightarrow$	$(1–\alpha)\times k_2$	(varied, this work)
(R2b)	$HO_2+CH_3C(O)CH_2O_2 \rightarrow OH+CH_3CO$	$\alpha\times k_2$	(varied, this work)
(R24)	$Cl+CH_3C(O)CH_3 \rightarrow CH_3C(O)CH_2$	2.1×10^{-12}	
(R27)	$OH+CH_3C(O)CH_3 \rightarrow CH_3C(O)CH_2$	1.8×10^{-13}	
(R25)	$CH_3C(O)CH_2+O_2 \rightarrow CH_3C(O)CH_2O_2$	1×10^{-12}	
	$CH_3C(O)CH_2+Cl_2 \rightarrow Cl$	4.3×10^{-11}	(estimate)
(R29a)	$2CH_3C(O)CH_2O_2 \rightarrow 2CH_3CO$	$0.63\times8\times10^{-12}$	
(R29b)	$2CH_3C(O)CH_2O_2 \rightarrow$	$0.37\times8\times10^{-12}$	
(R8a)	$HO_2+HOCH_2CH_2O_2 \rightarrow$	$(1-\alpha_8)\times1.4\times10^{-11}$	(varied, this work)
(R8b)	$HO_2+HOCH_2CH_2O_2 \rightarrow OH+O_2+HOCH_2CH_2O$	$\alpha_8\times1.4\times10^{-11}$	(varied, this work)
(R30a)	$Cl+CH_3CH_2OH \rightarrow CH_3CHOH+HCl$	$0.92\times8.6\times10^{-11}$	
(R30b)	$Cl+CH_3CH_2OH \rightarrow CH_2CH_2OH$	$0.08\times8.6\times10^{-11}$	
(R31)	$CH_3CHOH+O_2 \rightarrow HO_2+CH_3CHO$	1.9×10^{-11}	

note – all rate parameters taken from (Atkinson et al., 2007) unless stated.

(R32)	$CH_2CH_2OH+O_2+M \rightarrow HOCH_2CH_2O_2+M$	3.0×10^{-12}	
	$CH_3CHOH+Cl_2 \rightarrow Cl$	3×10^{-11}	(estimate)
	$CH_2CH_2OH+Cl_2 \rightarrow Cl$	3×10^{-11}	(estimate)
	$OH+CH_3CH_2OH \rightarrow CH_3CHOH$	$3.0\times10^{-12}\times\exp(20/T)$	
	$2HOCH_2CH_2O_2 \rightarrow$	$0.5 \times 7.8\times10^{-14}\times \exp(1000/T)$	
	$2HOCH_2CH_2O_2 \rightarrow 2HOCH_2CH_2O$	$0.5 \times 7.8\times10^{-14}\times \exp(1000/T)$	
(R9a)	$HO_2+CH_3CH(OH)CH_2O_2 \rightarrow$	$(1\text{-}\alpha_9)\times1\times10^{-11}$	(estimate, this work)
(R9b)	$HO_2+CH_3CH(OH)CH_2O_2 \rightarrow OH$	$\alpha_9 * 1\times10^{-11}$	(estimate, this work)
	$Cl+(CH_3)_2CHOH \rightarrow (CH_3)_2COH$	$0.85 \times 8.6\times10^{-11}$	(Yamanaka et al., 2007)
	$Cl+(CH_3)_2CHOH \rightarrow CH_3CH(OH)CH_2$	$0.15 \times 8.6\times10^{-11}$	(Yamanaka et al., 2007)
	$(CH_3)_2COH+O_2 \rightarrow HO_2$	1.9×10^{-11}	
	$CH_3CH(OH)CH_2+O_2 \rightarrow CH_3CH(OH)CH_2O_2$	1×10^{-11}	(estimate)
	$CH_3CH(OH)CH_2O_2+CH_3CH(OH)CH_2O_2 \rightarrow$	2×10^{-12}	(estimate)
	$OH+(CH_3)_2CHOH \rightarrow CH_3C(OH)CH_2$	5.1×10^{-12}	
(R33–36)	$HO_2+RO_2 \rightarrow$	$(1\text{-}\alpha)\times 1\times10^{-11}$	(estimate, this work)
(R33–36)	$HO_2+RO_2 \rightarrow OH$	$\alpha\times1\times10^{-11}$	(estimate, this work)
	$Cl+C_5H_8 \rightarrow R$	3.4×10^{-10}	(Bedjanian et al., 1998)
	$OH+C_5H_8 \rightarrow R$	1.0×10^{-10}	
	$Cl+(CH_3)_2CH(CH_2)_2OH \rightarrow R$	$0.5 \times 2.5\times10^{-10}$	(estimate, Wu et al., 2003)
	$Cl+(CH_3)_2CH(CH_2)_2OH \rightarrow HO_2$	$0.5 \times 2.5\times10^{-10}$	(estimate, Wu et al., 2003)
	$OH+(CH_3)_2CH(CH_2)_2OH \rightarrow R$	1.4×10^{-11}	(Wu et al., 2003)
	$Cl+C_6H_5CHO \rightarrow R$	9.6×10^{-11}	(Noziere et al., 1994)
	$OH+C_6H_5CHO \rightarrow R$	1.3×10^{-11}	(Baulch et al., 1994)
	$Cl+CH_3C(O)C_2H_5 \rightarrow R$	3.6×10^{-11}	
	$OH+CH_3C(O)C_2H_5 \rightarrow R$	1.2×10^{-12}	
	$R+O_2 \rightarrow RO_2$	6×10^{-12}	(estimate)
	$R+Cl_2 \rightarrow Cl$	3×10^{-11}	(estimate)
	$RO_2+RO_2 \rightarrow$	5×10^{-12}	(estimate)

Acknowledgements. The authors particularly wish to thank Mike Jenkin, Domenico Taraborelli, and Jonathan Williams, together with whole MPI GABRIEL team for their helpful suggestions. TJD acknowledges the receipt of a research Stipendium from the Max Planck Society.

Edited by: R. Cohen

The publication of this article is financed by the Max Planck Society.

References

Andersen, M. P. S., Hurley, M. D., Wallington, T. J., Ball, J. C., Martin, J. W., Ellis, D. A., and Mabury, S. A.: Atmospheric chemistry of C_2F_5CHO: mechanism of the $C_2F_5C(O)O_2+HO_2$ reaction, Chem. Phys. Lett., 381, 14–21, 2003.

Atkinson, R. and Arey, J.: Gas-phase tropospheric chemistry of biogenic volatile organic compounds: a review, Atmos. Environ., 37, S197–S219, 2003.

Atkinson, R., Baulch, D. L., Cox, R. A., Crowley, J. N., Hampson, R. F., Hynes, R. G., Jenkin, M. E., Kerr, J. A., Rossi, M. J., and Troe, J.: IUPAC Subcommittee for gas kinetic data evaluation. Evaluated kinetic data: http://www.iupac-kinetic.ch.cam.ac.uk/, 2007.

Bailey, A. E., Heard, D. E., Paul, P. H., and Pilling, M. J.: Collisional quenching of OH ($A^2\Sigma^+$, ν'=0) by N_2, O_2 and CO_2 between 204 and 294 K. Implications for atmospheric measurements of OH by laser-induced fluorescence, Journal of the Chemical Society-Faraday Transactions, 93, 2915–2920, 1997.

Baulch, D. L., Cobos, C. J., Cox, R. A., Frank, P., Hayman, G., Just, T., Kerr, J. A., Murrells, T., Pilling, M. J., Troe, J., Walker, R. W., and Warnatz, J.: Evaluated Kinetic Data For Combustion Modeling Supplement-I, J. Phys. Chem. Ref. Data, 23, 847–1033, 1994.

Bedjanian, Y., Laverdet, G., and Le Bras, G.: Low-pressure study of the reaction of Cl atoms with isoprene, J. Phys. Chem. A, 102, 953–959, 1998.

Bridier, I., Veyret, B., Lesclaux, R., and Jenkin, M. E.: Flash-Photolysis Study of the Uv Spectrum and Kinetics of Reactions of the Acetonylperoxy Radical, Journal of the Chemical Society-Faraday Transactions, 89, 2993–2997, 1993.

Carr, S. A., Baeza-Romero, M. T., Blitz, M. A., Pilling, M. J., Heard, D. E., and Seakins, P. W.: OH yields from the CH_3CO+O_2 reaction using an internal standard, Chem. Phys. Lett., 445, 108–112, 2007.

Crawford, M. A., Wallington, T. J., Szente, J. J., Maricq, M. M., and Francisco, J. S.: Kinetics and mechanism of the acetylperoxy plus HO_2 reaction, J. Phys. Chem. A, 103, 365–378, 1999.

Curtis, A. R. and Sweetenham, W. P.: Facsimile, AERE, Report R-12805, 1987.

Dillon, T. J., Hölscher, D., Sivakumaran, V., Horowitz, A., and Crowley, J. N.: Kinetics of the reactions of HO with methanol (210–351 K) and with ethanol (216–368 K), Phys. Chem. Chem. Phys., 7, 349–355, 2005.

Dillon, T. J., Horowitz, A., and Crowley, J. N.: Absolute rate coefficients for the reactions of $O(^1D)$ with a series of n-alkanes, Chem. Phys. Lett., 14, 12–16, 2007.

Dillon, T. J., Horowitz, A., Hölscher, D., and Crowley, J. N.: Reaction of HO with hydroxyacetone ($HOCH_2C(O)CH_3$): rate coefficients and mechanism., Phys. Chem. Chem. Phys., 8, 236–246, 2006a.

Dillon, T. J., Tucceri, M. E., and Crowley, J. N.: Laser induced fluorescence studies of IO kinetics, part 2: Reaction of IO with CH_3O_2, CF_3O_2 and O_3 at 298 K, Phys. Chem. Chem. Phys., 8, 5185–5198, 2006b.

Dillon, T. J., Tucceri, M. E., Sander, S., and Crowley, J. N.: LIF studies of iodine oxide chemistry, part 3. Reactions $IO+NO_3=OIO+NO_2$, $I+NO_3=IO+NO_2$, and CH_2I+O_2=(products): Implications for the chemistry of the marine atmosphere at night., Phys. Chem. Chem. Phys., 10, 1540–1554, 2008.

Gierczak, T., Gilles, M. K., Bauerle, S., and Ravishankara, A. R.: Reaction of hydroxyl radical with acetone. 1. Kinetics of the reactions of OH, OD, and ^{18}O with acetone and acetone-D_6, J. Phys. Chem. A, 107, 5014–5020, 2003.

Hasson, A. S., Kuwata, K. T., Arroyo, M. C., and Petersen, E. B.: Theoretical studies of the reaction of hydroperoxy radicals (HO_2 center dot) with ethyl peroxy ($CH_3CH_2O_2$ center dot), acetyl peroxy ($CH_3C(O)O_2$(center dot)) and acetonyl peroxy ($CH_3C(O)CH_2O_2$ center dot) radicals, J. Phtochem. Photobiol. A Chemistry, 176, 218–230, 2005.

Hasson, A. S., Tyndall, G. S., and Orlando, J. J.: A product yield study of the reaction of HO_2 radicals with ethyl peroxy ($C_2H_5O_2$), acetyl peroxy ($CH_3C(O)O_2$), and acetonyl peroxy ($CH_3C(O)CH_2O_2$) radicals, J. Phys. Chem. A, 108, 5979–5989, 2004.

Horie, O. and Moortgat, G. K.: Reactions of $CH_3C(O)O_2$ Radicals with CH_3O_2 and HO_2 between 263 and 333-K – a Product Study, Journal of the Chemical Society-Faraday Transactions, 88, 3305–3312, 1992.

Jenkin, M. E., Hurley, M. D., and Wallington, T. J.: Investigation of the radical product channel of the $CH_3C(O)O_2+HO_2$ reaction in the gas phase, Phys. Chem. Chem. Phys., 9, 3149–3162, 2007.

Jenkin, M. E., Hurley, M. D., and Wallington, T. J.: Investigation of the radical product channel of the $CH_3C(O)CH_2O_2+HO_2$ reaction in the gas phase, Phys. Chem. Chem. Phys., 10, 4274–4280, 2008.

Karunanandan, R., Hölscher, D., Dillon, T. J., Horowitz, A., and Crowley, J.: Reaction of HO with glycolaldehyde, $HOCH_2CHO$: Rate coefficients (240–362 K) and mechanism, J. Phys. Chem. A, 111, 897–908, 2007.

Le Crane, J. P., Rayez, M. T., Rayez, J. C., and Villenave, E.: A reinvestigation of the kinetics and the mechanism of the $CH_3C(O)O_2+HO_2$ reaction using both experimental and theoretical approaches, Phys. Chem. Chem. Phys., 8, 2163–2171, 2006.

Lelieveld, J., Butler, T. M., Crowley, J. N., Dillon, T. J., Fischer, H., Ganzeveld, L., Harder, H., Lawrence, M. G., Martinez, M., Taraborrelli, D., and Williams, J.: Atmospheric oxidation capacity sustained by a tropical forest, Nature, 452, 737–740, 2008.

Lightfoot, P. D., Cox, R. A., Crowley, J. N., Destriau, M., Hayman, G. D., Jenkin, M. E., Moortgat, G. K., and Zabel, F.: Organic peroxy radicals: kinetics, spectroscopy and tropospheric chemistry, Atmos. Environ., 264, 1805–1964, 1993.

Moortgat, G. K., Veyret, B., and Lesclaux, R.: Kinetics of the Reaction of HO_2 with $CH_3C(O)O_2$ in the Temperature-Range 253-K-368-K, Chem. Phys. Lett., 160, 443–447, 1989.

Niki, H., Maker, P. D., Savage, C. M., and Breitenbach, L. P.: Ftir Study of the Kinetics and Mechanism For Cl-Atom-Initiated Reactions of Acetaldehyde, J. Phys. Chem., 89, 588–591, 1985.

Noziere, B., Lesclaux, R., Hurley, M. D., Dearth, M. A., and Wallington, T. J.: A Kinetic and Mechanistic Study of the Self-Reaction and Reaction with HO_2 of the Benzylperoxy Radical, J. Phys. Chem., 98, 2864–2873, 1994.

Salahub, D. R., and Sandorfy, C.: Far-Ultraviolet Spectra of Some Simple Alcohols and Fluoroalcohols, Chem. Phys. Lett., 8, 71–74, 1971.

Thornton, J. A., Wooldridge, P. J., Cohen, R. C., Martinez, M., Harder, H., Brune, W. H., Williams, E. J., Roberts, J. M., Fehsenfeld, F. C., Hall, S. R., Shetter, R. E., Wert, B. P., and Fried, A.: Ozone production rates as a function of NOx abundances and HOx production rates in the Nashville urban plume, J. Geophys. Res., 107(D12), 4146, doi:10.1029/2001JD000932, 2002.

Tomas, A., Villenave, E., and Lesclaux, R.: Reactions of the HO_2 radical with CH_3CHO and $CH_3C(O)O_2$ in the gas phase, J. Phys. Chem. A, 105, 3505–3514, 2001.

Tyndall, G. S., Cox, R. A., Granier, C., Lesclaux, R., Moortgat, G. K., Pilling, M. J., Ravishankara, A. R., and Wallington, T. J.: Atmospheric chemistry of small organic peroxy radicals, J. Geophys. Res., 106, 12 157–12 182, 2001.

Tyndall, G. S., Orlando, J. J., Kegley-Owen, C. S., Wallington, T. J., and Hurley, M. D.: Rate coefficients for the reactions of chlorine atoms with methanol and acetaldehyde, Int. J. Chem. Kin., 31, 776–784, 1999.

Wollenhaupt, M., Carl, S. A., Horowitz, A., and Crowley, J. N.: Rate coefficients for reaction of OH with acetone between 202 and 395 K, J. Phys. Chem. A, 104, 2695–2705, 2000.

Wu, H., Mu, Y. J., Zhang, X. S., and Jiang, G. B.: Relative rate constants for the reactions of hydroxyl radicals and chlorine atoms with a series of aliphatic alcohols, Int. J. Chem. Kin., 35, 81–87, 2003.

Yamanaka, T., Kawasaki, M., Hurley, M. D., Wallington, T. J., Schneider, W. F., and Bruce, J.: Kinetics and mechanism of the gas phase reaction of chlorine atoms with i-propanol, Phys. Chem. Chem. Phys., 9, 4211–4217, 2007.